

4. Dowling K, Dayel MJ, Lever MJ, French PMW, Hares JD, Dymoke-Bradshaw AKL (1998) Fluorescence lifetime imaging with picosecond resolution for biomedical applications. *Optics Letters* 23(10):810–812
5. Lakowicz JR, Berndt KW (1991) Lifetime-selective fluorescence imaging using an rf phase-sensitive camera. *Rev Sci Instrum* 62(7):1727–1734
6. Clegg RM, Feddersen B, Gratton E, Jovin TM (1992) Time resolved imaging fluorescence microscopy. *SPIE* 1640:448–460
7. Morgan CG, Mitchell AC, Murray JG (1992) In-situ fluorescence analysis using nanosecond decay time imaging. *Trends Anal Chem* 11(1):32–41
8. Gadella TWJ, Jovin TM, Clegg RM (1993) Fluorescence lifetime imaging microscopy (FLIM): spatial resolution of microstructures on the nanosecond time scale. *Biophys Chem* 48:221–239
9. Verveer PJ, Squire A, Bastiaens PIH (2000) Global analysis of fluorescence lifetime imaging microscopy data. *Biophys J* 78:2127–2137
10. Neumann M, Herten DP, Dietrich A, Wolfrum J, Sauer M (2000) Capillary array scanner for time-resolved detection and identification of fluorescently labelled DNA fragments. *J Chromatography A* 871:299–310
11. Lassiter SJ, Stryjewski W, Legendre BL, Erdman R, Wahl M, Wurm J, Peterson R, Middendorf L, Soper SA (2000) Time-resolved fluorescence imaging of slab gels for lifetime base-calling in DNA sequencing applications. *Anal Chem* 72:5373–5382
12. Piston DW, Sandison DR, Webb WW (1992) Time-resolved fluorescence imaging and background rejection by two-photon excitation in laser scanning microscopy. *SPIE* 1640:379–390
13. Dong CY, So PTC, French T, Gratton E (1995) Fluorescence lifetime imaging by asynchronous pump-probe microscopy. *Biophys J* 69:2234–2242
14. Buurman EP, Sanders R, Draaijer A, Gerritsen HC, van Veen JJF, Hout PM, Levine YK (1992) Fluorescence lifetime imaging using a confocal laser scanning microscope. *Scanning* 14:155–159
15. Vroom JM, de Grauw KJ, Gerritsen HC, Bradshaw DJ, Marsh PD, Watson GK, Birmingham JJ, Allison C (1999) Depth penetration and detection of pH gradients in biofilms by two-photon excitation microscopy. *Appl Env Micro* 65(8):3502–3511
16. Abramowitz M, Stegun IA (1965) *Handbook of mathematical functions*. Dover, New York, p 80, formula 4.4.10
17. Haykin S (1983) *Communication Systems*. J Wiley, New York, pp 364–371
18. Blackman RB, Tukey JW (1959) *The measurement of power spectra from the point of view of communications engineering*. Dover, New York, pp 31–33
19. Boas ML (1983) *Mathematical methods in the physical sciences*. J Wiley, New York, pp 81–95
20. Birmingham JJ (1997) Frequency-domain lifetime imaging methods at Unilever Research. *J Fluorescence* 7(1):45–54
21. Wilson T, Neil MAA, Juskaitis R (1998) Real-time three-dimensional imaging of macroscopic structures. *J Microscopy* 191(2):116–118
22. Neil MAA, Squire A, Juskaitis R, Bastiaens PIH, Wilson T (2000) Wide-field optically sectioning fluorescence microscopy with laser illumination. *J Microscopy* 197(1):1–4
23. Tweed DG (1984) Resonant scanner linearization techniques. *SPIE* 498:161–168
24. Harris P, Sipior J, Ram N, Carter GM, Rao G (1999) *Rev Sci Instrum* 70(2):1535–1539

Spectral Imaging of Single CdSe/ZnS Quantum Dots Employing Spectrally- and Time-resolved Confocal Microscopy

W.G.J.H.M. VAN SARK, P.L.T.M. FREDERIX, M.A.H. ASSELBERGS, D.J. VAN DEN HEUVEL, A. MEIJERINK, AND H. C. GERRITSEN

A spectrally- and time-resolved study of single CdSe/ZnS quantum dots (QDs) is presented. To this end a versatile, high sensitivity spectrograph is coupled to a confocal laser-scanning microscope. The spectrograph is built in-house and is especially developed for use in fluorescence microscopy. The high sensitivity is achieved by using a prism for the dispersion of light in combination with a state-of-the-art back-illuminated charge-coupled device (CCD) camera. The detection efficiency of the spectrograph, including the CCD camera, amounts to 0.77 ± 0.05 at 633 nm. Full emission spectra with a 1–5 nm spectral resolution can be recorded at a maximum rate of 800 spectra per second. The spectrograph can easily be fiber-coupled to any confocal laser-scanning microscope.

The spectral characteristics of the QDs are studied in two different ambi-ents: air and nitrogen. For QDs in ambient air, a clear 30 nm blue-shift in the emission wavelength is observed, before the luminescence stops after about 2–3 minutes due to photobleaching. In a nitrogen atmosphere, the blue shift is absent while photobleaching occurs after much longer times, i.e., 10–15 minutes. These observations are explained by photo-induced oxidation. The CdSe surface is oxidized during illumination in the presence of oxygen. This effectively results in shrinkage of the CdSe core diameter by almost 1 nm, and consequently in a blue shift. The faster fading of the luminescence in air suggests that photo-induced oxidation results in the formation of non-radiative recombination centers at the CdSe/CdSeO_x interface. In a nitrogen atmosphere photo-induced oxidation is prevented by the absence of oxygen. Additionally, a higher initial light output for CdSe/ZnS QDs in air is observed. This can be explained by a reduction of the lifetime of the long-lived defect states of CdSe QDs by oxygen.

19.1 Introduction

Nanometer-sized semiconductor quantum dots (QDs) nowadays are extensively studied [1–4]. The change in the electronic structure as a function of QD-size is most evident from the variation of their emission wavelength [2, 5–7], and is the basis for many new applications in physics, chemistry, and biology, see, e.g., [8]. Due to the confinement of electrons and holes in the nanocrystallites the energy-level scheme resembles that of an atom, with many discrete energy levels. The separation between energy levels increases as the particle size decreases. As an example, the radius of the bulk Bohr exciton amounts to 5.6 nm for CdSe [6], hence nanocrystallites with a size smaller than the Bohr radius, will show quantum confinement effects. Dabbousi et al. have shown that CdSe QDs with a diameter of 2.3 nm fluoresce at 470 nm, and QDs with a diameter of 5.5 nm fluoresce at 610 nm [5]. Capping of CdSe QDs with a few monolayers of ZnS increases the quantum efficiency considerably to values exceeding 50% [9, 10].

The tunability of the optical properties of QDs by changing their size also makes them difficult to study. A prerequisite for the study of QDs is the ability to produce them with a narrow size distribution (< 5%). Variations of size and shape within ensemble samples result in extensive inhomogeneous broadening of absorption and emission spectra. Measuring spectra of *single* QDs can circumvent these effects. Since Blanton et al. [11] and Nirmal et al. [12] showed that it is possible to measure *single* QD emission spectra, the study of the luminescence of single semiconductor QDs has revealed many interesting properties that cannot be observed for an ensemble of QDs. Phenomena of fundamental interest such as spectral diffusion and blinking (on–off behavior [13, 14]) are also important for potential applications of single quantum dots as luminescent labels in biological systems [10, 15–17].

Most studies on spectral diffusion have been performed at cryogenic temperatures. Random spectral diffusion at low temperatures has been related to blinking and therefore the ionization of quantum dots due to Auger processes [12–14, 18–20]. As a result of the ionization and subsequent recombination processes, the charge distribution around the QD changes, resulting in a spectral (Stark) shift of the emission [20, 21]. A clear relation between blinking (explained by photo-ionization) and the occurrence of a spectral jump has been established. At room temperature less information is available on spectral diffusion of single QD luminescence. A non-random blue shift of about 10–15 nm has been reported [12, 22], which was attributed to photo-oxidation of the quantum dot.

The measurement of *single* QD emission spectra is just one example of the many applications in fluorescence microscopy that require multiple wavelength band detection. Other examples include the simultaneous imaging of multiple probes in morphological studies, the quantification of ion concentrations using the ratio of the fluorescence signal in two emission bands imaging [23], the measurement of nanometer co-localization by means of Förster Resonance Energy Transfer (FRET) [24] and the very recently observed FRET between QDs and organic dyes [25, 26].

A common and simple way to implement the detection of multiple wavelength bands is the use of multiple emission filters. However, in general the bandwidth of the emission filters is comparatively broad and the number of wavelength bands used in the imaging experiment is limited. The number of wavelength bands that can be detected (simultaneously) limits the number of parameters that can be monitored. Importantly, the broad emission bands of organic fluorescent probes often overlap. This complicates the separation of multiple spectra. Moreover, the broad detection bandwidth and limited number of detection channels do not allow assessment of the shapes of the emission spectra. Therefore, no direct indication of unexpected spectral shifts or the presence of artifacts such as auto-fluorescence or scattered excitation light is present in the images. This may result in the misinterpretation of the observed intensities.

The measurement of complete emission spectra under the microscope can be used to solve these problems [27–34]. However, the acquisition of reliable emission spectra requires the detection of a large number of photons. This restricts both the acquisition rate of the images and the number of images that can be recorded before a fluorescent probe is photobleached.

In this chapter we describe a highly sensitive spectrograph that is optimized for use in (scanning) fluorescence microscopy. The high sensitivity is achieved by using a prism for the dispersion in combination with a back illuminated CCD camera. Complete emission spectra with a 1–5 nm resolution can be recorded with millisecond dwell times. The spectrograph is connected to a commercial confocal laser-scanning microscope (CLSM). Several of its unique features will be elucidated in a time-resolved study at room-temperature of emission spectra of *single* CdSe/ZnS QDs.

19.2 Experimental

19.2.1 Spectrograph-CLSM Set-up

19.2.1.1 Description

The spectrograph was designed and constructed in-house. Two important design parameters were the wavelength range and the spectral resolution. As the spectrograph was intended for use in biological studies, they were set to 450–750 nm, and 1–5 nm, respectively. Furthermore, reasonable spectral imaging acquisition times require short integration times per spectrum. In a scanning microscope, dwell times per pixel of up to a few milliseconds were considered acceptable. Another important consideration was the detection efficiency, as in fluorescent microscopy only a limited number of fluorescent probes are present per pixel, i.e., ranging from one to several hundreds. This limits the number of available photons. Also photobleaching effects will reduce the number of photons. Finally, in order to re-

cord a reliable emission spectrum a comparably large amount of photons are to be detected. Further detailed design considerations can be found elsewhere [35, 36]. On the basis of these considerations a back-illuminated CCD camera was chosen as the detector, and an antireflection-coated prism as the dispersive element.

For flexibility reasons the entrance of the spectrograph was equipped with a standard multimode fiber adaptor. Light emerging from the fiber (or directly coupled light) was collimated by a 100 mm F/2.5 achromatic lens (Melles-Griot). Next, the light was dispersed by the prism and focused on the CCD camera by an identical lens. Note that the fiber end was projected on the camera without magnification.

An equilateral SF10-glass prism (Linos), operating at minimum deviation conditions, dispersed the light. The minimum deviation wavelength was chosen at 550 nm. For this wavelength the angle of incidence at the entrance surface equaled the angle of emergence at the exit surface. For the prism employed here, this yielded an entrance angle of 60.1 degrees. The interfaces of the prism were coated with a single layer MgF₂-coating, to enhance the transmission. The lengths of the legs of the prism (60 mm) limited the numerical aperture of the spectrograph. The usable prism width was slightly (i.e., about 1 mm) diminished by the fact that the dispersed beam was wider than the beam before dispersion. From the focal length of the collimating lens and the length of the legs of the prism a maximum numerical aperture of 0.14 was found for the beam of light entering the spectrograph.

The spectrograph was equipped with a Peltier cooled, back-illuminated CCD camera (Princeton Instruments NTE/CCD-1340, 16 bit ST133 controller, readout noise 6e⁻ at 1 MHz ADC). The CCD chip was 1340 pixels long in the dispersion direction (horizontal) and 100 pixels high (vertical) and had 20×20 μm² square pixels. The spectral measurements were carried out on a small sub-area of the CCD chip of less than 10 pixels high and between 50 and 400 pixels long. The pixels in the direction perpendicular to the dispersion direction were always hardware binned. Moreover, hardware binning can be employed in the dispersion direction as well, albeit at the price of a loss of spectral resolution. To gain speed, the sub-area was positioned at the corner of the CCD-chip closest to the readout amplifier. To facilitate alignment of the CCD-chip it was mounted on two orthogonal translation stages. In order to select another wavelength region the camera was simply translated with respect to the prism.

The experiments presented here were all recorded using a confocal laser-scanning microscope (CLSM, Nikon PCM2000, in combination with a Nikon Optiphot 2 microscope). The CSLM scan head was equipped with a standard single-mode fiber adaptor for excitation and two multimode fiber adapters for coupling the emission light to the (remote) detectors. The first of the two detection channels was coupled to the spectrograph. A schematic diagram of the set-up is shown in Fig. 19.1.

A 50 μm core diameter fiber patch cord equipped with standard connectors on both ends (Thorlabs, FG-050-GLA) was used to interface the spectrograph to the CLSM. Because of the comparatively large fiber core diameter of 50 μm, the alignment of the fiber was not critical. The fiber adapter at the CLSM was manually adjusted to optimize the fluorescence signal. Furthermore, the numerical aper-

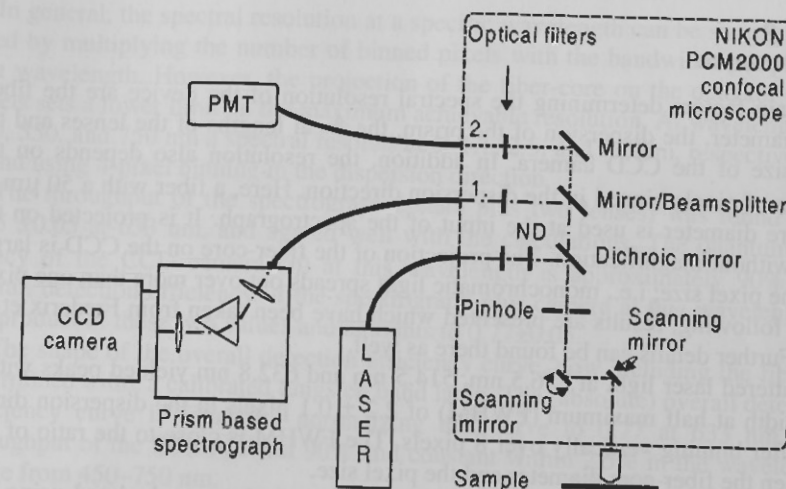


Fig. 19.1. Schematic overview of the experimental set-up. The excitation light from the mixed gas Argon-Krypton laser is guided to the CLSM by a single mode fiber. An excitation filter and a neutral density filter (ND) can be placed in the excitation beam. Each of the two emission paths can be equipped with a longpass or bandpass emission filter. Detection channel 1 of the CLSM is connected to the spectrograph and channel 2 is connected to a PMT. Channel 1 and 2 are selected by the insertion of a mirror or beamsplitter in the emission path, respectively. The lenses of the CLSM are omitted from the picture for clarity.

ture of the light emerging from the CLSM (< 0.12) and that of the spectrograph (0.14) were reasonably matched. This ensures efficient coupling of the two devices.

The pixel clock pulses generated by the CLSM were used to synchronize the CLSM and the CCD camera controller. The CLSM was used for acquiring 2D spectral images (2D-mode) or for time resolved spectral analysis of small volume elements (time-mode). The wavelength, the confocal pinhole size, the objective magnification and the numerical aperture of the objective determine the spatial resolution. The measurements discussed below, were carried out with a 60× oil immersion objective (Nikon PlanApo 1.4 NA) and with the larger of two available pinholes (50 μm). The axial and lateral resolutions were estimated to be approximately 1 μm and 0.3 μm, respectively.

The Argon-Krypton mixed gas laser (Spectra Physics, 2060-10SA) used here provides a large number of excitation wavelengths (400–650 nm). A single mode fiber guided the laser light to the CLSM. The excitation light was reflected towards the sample by the built-in dichroic mirror of the confocal microscope (Nikon). Typical laser powers at the sample ranged from 1–100 μW.

19.2.1.2 Performance

The main factors determining the spectral resolution of the device are the fiber-core diameter, the dispersion of the prism, the focal lengths of the lenses and the pixel size of the CCD camera. In addition, the resolution also depends on the number of pixels binned in the dispersion direction. Here, a fiber with a 50 μm fiber-core diameter is used at the input of the spectrograph. It is projected on the CCD without magnification. The projection of the fiber-core on the CCD is larger than the pixel size; i.e., monochromatic light spreads out over more than one pixel. In the following, results are presented which have been taken from Frederix et al. [35]. Further details can be found there as well.

Scattered laser light at 476.5 nm, 514.5 nm and 632.8 nm yielded peaks with a full width at half maximum (FWHM) of 2.2 ± 0.1 pixels in the dispersion direction after binning vertically over 8 pixels. The FWHM is close to the ratio of 2.5 between the fiber-core diameter and the pixel size.

The non-linear spectral bandwidth per camera pixel was calculated using the angular dispersion of the prism [37], the focal length of the second lens, the camera pixel size. This pixel bandwidth is shown in Fig. 19.2. The spectrograph is operated at a fixed geometry of the prism and lenses. Therefore the shape of the wavelength calibration curve is constant. The calibration of the spectrograph was accomplished by fitting the measured CCD pixel positions of a number of calibration lines (3 or more) to the theoretical expression of the calibration curve. An additional scaling factor was included in the fit to account for errors in the magnification of the spectrograph. Calibration measurements were carried out with laser lines or with a calibration lamp (HgAr lamp, Oriel), depending on the wavelength range of interest. The peak positions were determined using the Winspec-software of the CCD camera (Princeton Instruments). Typically, the calibration accuracy was better than 1 nm over the whole wavelength range.

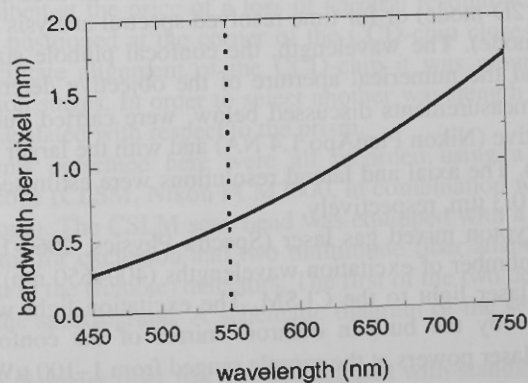


Fig. 19.2. Pixel bandwidth of the spectrograph, plotted against the wavelength. The vertical dotted line at 550 nm denotes the minimum deviation wavelength of the prism

In general, the spectral resolution at a specific wavelength can be simply calculated by multiplying the number of binned pixels with the bandwidth per pixel at that wavelength. However, the projection of the fiber-core on the detector of 2.2 pixels sets a lower limit on the maximum achievable resolution. At wavelengths of 450, 550, and 750 nm a spectral resolution of 1.1, 2.5, and 7.0 nm, respectively, is found using 4-pixel binning in the dispersion direction.

The throughput of the spectrograph (prism plus two lenses) was found to be 0.85 ± 0.05 at 633 nm, and agreed well with the calculations. The quantum efficiency of the CCD camera (η) at this wavelength is approximately 90%. The overall detection efficiency of the spectrograph plus camera at this wavelength is the product of these two values and amounts to 0.77 ± 0.05 .

The shape of the overall detection efficiency curve, now including the fiber, is determined using a calibrated tungsten band lamp. The (absolute) overall detection efficiency curve is found by normalizing this curve to 0.77 at 633 nm. The throughput of the fiber is about 90% and constant within 2.5% in the wavelength range from 450–750 nm.

The CCD camera has a maximum rate of approximately 800 spectra (of 20–100 points/spectrum) per second at a $N_{RD} = 6 e^-$. Therefore, pixel dwell times in excess of 1.2 ms were employed. In 2D-mode, a 160×160 points image with 1.2 ms dwell time is recorded in approximately 40 seconds. Due to the time lost during the retrace of the mirror, the acquisition time is somewhat longer than the number of spectra multiplied by the dwell time.

The internal timing of the camera can be modified to increase the maximum spectral rate, at the price of extra noise. Alternatively a slow ADC (100 kHz) can be employed to reduce the N_{RD} to $3.5 e^-$. However, this decreases the maximum spectral rate.

Measurements were carried out using two PCs both running Windows 98 (Microsoft). The first PC controls the CLSM and the second controls the CCD camera. The Microsoft automation server and automation manager were used to synchronize the start of the recording of spectra by the CCD camera and of the scanning. To this end the operating software of the CLSM (EZ2000 Nikon, Coord automatisering) was slightly modified. Acquisition of the spectra was carried out using the Winspec-software that controls the CCD camera and raw data are saved to disk.

For each point in a 2D-image a whole emission spectrum was recorded. Consequently, 3D data sets were created (x, y, λ). Data processing and visualization of the 3D data sets were carried out with a program written for use in IDL (Creaso). The program subtracts a (user-defined) background from the raw spectra and corrects for the detection efficiency of the set-up. The wavelength calibration was performed as explained above. Where possible, the average spectrum from an area in the image with no obvious fluorescence was employed as a background. If such an area was not available, a background spectrum from a comparable (reference) specimen was used. The wavelength dependency of the detection efficiency of the complete set-up was corrected for with a so-called 'flat-field' spectrum. The flat-field spectra were determined by using a calibrated tungsten band lamp. The band lamp spectrum was assumed to be identical to the spectrum of a black body radia-

tor of the same temperature. The flat-field spectrum was calculated from the ratio of the band lamp spectrum and the spectrum of the black body radiator. The flat-field spectrum also includes the variable bandwidth per CCD pixel. A more detailed description of the data correction can be found in [36]. Intensity images can be viewed at each recorded wavelength band. Furthermore, emission spectra from selected pixels, or regions of interest, can be viewed and exported for further analysis.

The data sets in time-mode are 2D (t, λ). The processing of these data sets was done in a similar way as described above. The background was taken from time intervals with no obvious fluorescence. If this was not available, a background spectrum from a comparable (reference) specimen was used.

19.2.2

QD Synthesis and Characterization

The ZnS-capped CdSe nanoparticles were synthesized by using a TOP/TOPO method similar to the one described by Hines and Guyot-Sionnest [9, 38, 39]. Two batches of overcoated dots were synthesized. For batch 1 about 4 monolayers of ZnS were grown over the CdSe core, while for batch 2 the thickness amounted to about 7 monolayers. The number of monolayers is based on the amounts of precursors used in the synthesis.

The synthesis was performed in a glovebox filled with nitrogen. Stock solutions of Cd, Zn, S and Se in TOP were prepared. For the Cd/TOP stock solution 1.6 g (0.011 mol) dimethylcadmium was dissolved in 15.5 mL TOP. The Zn/TOP stock solution was prepared by dissolution of 1.23 g (0.01 mol) diethylzinc in 9.0 mL TOP. 1.3 g Se (0.016 mol) was dissolved in 16.0 mL TOP and 2.0 mL (0.01 mol) $(\text{TMS})_2\text{S}$ was dissolved in 8.0 mL TOP to obtain the Se/TOP and S/TOP stock solutions, respectively. Cd/Se/TOP and Zn/S/TOP stock solutions were freshly prepared for every synthesis. The Cd/Se/TOP stock solution was prepared by diluting 0.4 mL Cd/TOP and 0.4 mL Se/TOP in 2.0 mL TOP. Dissolution of 1.6 mL S/TOP and 1.12 mL Zn/TOP in 8.28 mL TOP gave the Zn/S/TOP stock solution.

The synthesis was performed by the following method. 25 g TOPO was heated to 300°C and kept at this temperature for half an hour to degas and dry the TOPO. The temperature was raised to 370°C. The heater was then removed and the temperature dropped. At 360°C 1.4 mL Cd/Se/TOP stock solution (containing 0.13 mmol Cd and 0.20 mmol Se) was injected rapidly. The reaction mixture was allowed to cool to 300°C and at this temperature 5.5 mL of the Zn/S/TOP stock solution (0.62 mmol Zn, 0.88 mmol S) was added in five portions at approximately 20 s intervals (batch 1). For batch 2, 13.73 mL of the Zn/S/TOP was added in five portions. After this injection the reaction mixture was allowed to cool down to 100°C and was kept at this temperature for one hour. The nanocrystals were purified by precipitation with anhydrous methanol. The precipitate was collected by centrifuging (4000 rpm, 5 min). The precipitate was then washed three times with anhydrous methanol. The nanocrystals were dispersed in doubly distilled chloroform.

Absorption spectra were recorded using a double beam Perkin-Elmer Lambda 16 UV/VIS spectrophotometer. Electron microscopy was performed with a Philips CM300UT-FEG electron microscope operating at 300 kV. Emission and excitation spectra were recorded with a SPEX Fluorolog spectrofluorometer equipped with two double grating 0.22 m SPEX 1680 monochromators and a 450 W Xenon lamp as excitation source. The emission was detected with a cooled Hamamatsu R928 photomultiplier.

To determine the luminescence quantum efficiency of a sample the integrated emission intensity was compared to that of a reference solution with known quantum efficiency, i.e., sulphorhodamine 101 in ethanol with 90% quantum efficiency. If necessary the solutions were diluted in order to have an absorbance that is in the regime where the emission intensity scales linearly with the number of absorbed photons.

For single particle luminescence measurements, small droplets of a strongly diluted QD stock solution were deposited, spread out, and dried on cover glass slides. The final density was approximately 0.1 dot/ μm^2 . The slides were prepared, mounted and sealed in a flowchamber in nitrogen. Prior to and during the experiments nitrogen or air was flushed through the flowchamber.

Fast spectral imaging of single dots was performed employing the above described spectrograph-CLSM set-up. The 468 nm line of the Ar-Kr CW laser was used for excitation (power $\approx 20 \text{ kW/cm}^2$). The photomultiplier of the CLSM (channel 2 in Fig. 19.1) was first used to locate a single QD, applying a 590/60 bandpass filter (center transmission wavelength is at 590 nm, FWHM of the band is 60 nm). Subsequently, the laser beam was parked at the position of single QDs and spectra (range 500–700 nm) were recorded with a 6 ms dwell time using the spectrograph (channel 1 in Fig. 19.1). Four pixels were binned in the dispersion direction, yielding a spectral resolution of about 3 nm at 580 nm. A 480 nm long-pass filter (Ba480, Nikon) was inserted in the detection path to block scattered laser light.

The luminescence of QDs was followed until the luminescence had been bleached away. Data are corrected for the background signal from the system and sample as described above [35, 36]. Data are further corrected for the detection sensitivity of the set-up using a calibrated tungsten bandlamp. The spectra are fitted by a Lorentzian peak function [2] for quantification of the integrated intensity, the peak position, and the peak width.

19.3

Results and Discussion

A typical absorption spectrum of a sample of CdSe/ZnS quantum dots is shown in Fig. 19.3. Due to quantum size effects the absorption spectra of the CdSe/ZnS nanoparticles has shifted to the blue compared to the absorption spectrum of bulk CdSe (absorption onset around 730 nm [40]). The structure in the absorption band is a result of the formation of discrete energy levels caused by quantum size effects. The insert in Fig. 19.3 shows a histogram of the size distribution of batch 1

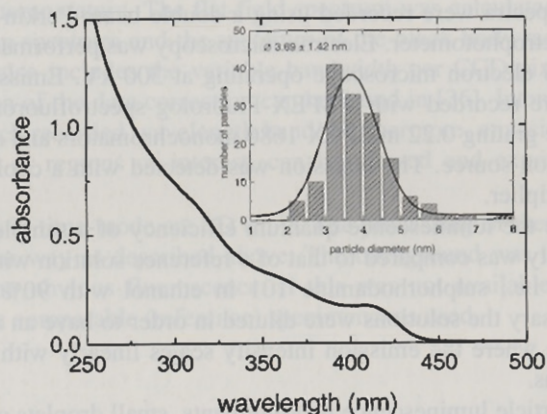


Fig. 19.3. UV-VIS absorption spectrum of CdSe QDs overgrown with 4 monolayers of ZnS (batch 1) as determined from HR-TEM photographs. The insert shows a histogram of the particle size distribution, revealing a ~50% polydispersity

obtained from HR-TEM pictures [39]. It was not possible to distinguish between the CdSe core and the ZnS shell on the HR-TEM pictures. For the histogram the size of 147 quantum dots was determined. The width of the size distribution of batch 1 is about 50%. The average particle diameter of the CdSe/ZnS core shell QDs is about 3.7 nm. For batch 2 similar results were obtained.

By spectral imaging of the CdSe/ZnS QDs with the spectrograph-CLSM set-up individual QDs and their emission spectra could easily be resolved. In Fig. 19.4 the spectra of a few of these QDs of batch 1 are shown, with emission wavelengths of 538, 562, 601, 619, and 640 nm, and FWHMs between 13 and 18 nm.

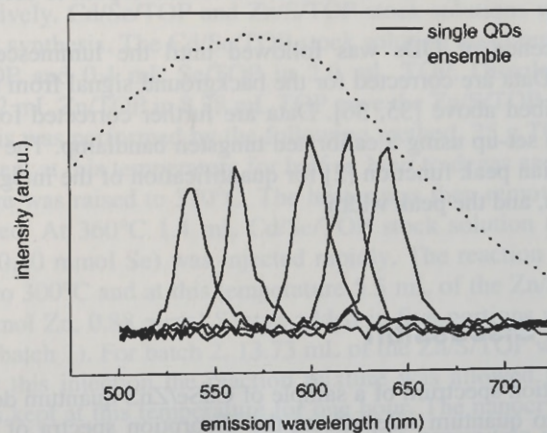


Fig. 19.4. Fluorescence emission spectra of several single QDs recorded with the spectrograph-CLSM set-up, compared to the spectrum of an ensemble of QDs. The emission wavelengths of the single QDs are 538, 562, 601, 619, and 640 nm (excitation wavelength 468 nm)

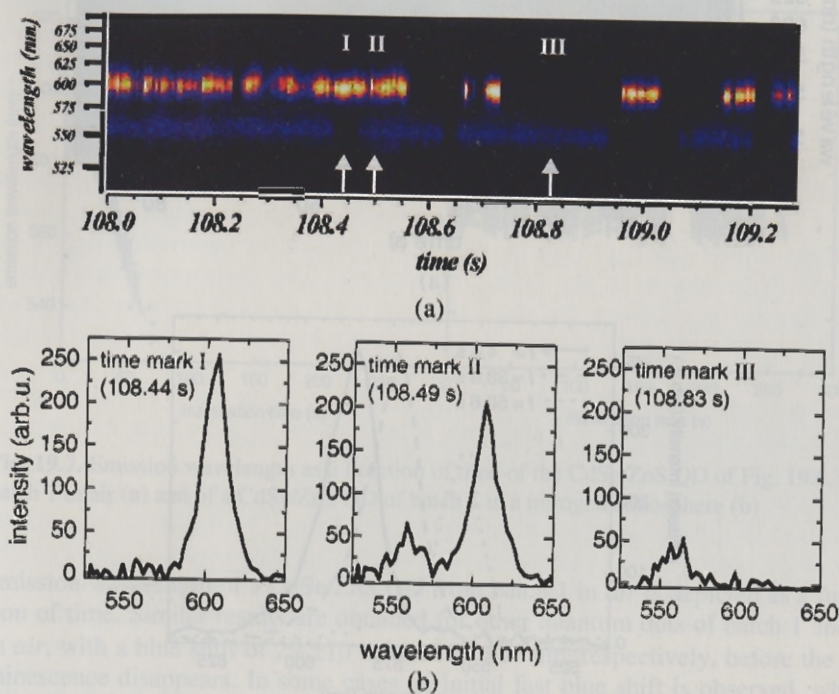


Fig. 19.5. a Spectrally resolved time trace (2.3 s) of two different QDs present in the detection volume of the spectrograph-CLSM set-up. The QDs can be separated due to their different emission wavelength, i.e., 605 and 560 nm, respectively. Complete spectra at times marked with I, II, and III are shown in b. Note that the intensity is a stretched false color representation

The corresponding diameters are 3.5, 4.1, 5.3, 6.1, and 7.1 nm, respectively, as calculated using the relation between diameter and emission wavelength [5]. The emission spectrum of the ensemble is shown for comparison. The value of the linewidth is in agreement with the homogeneous broadening at room temperature by phonon dephasing processes [41]. As a result of quantum confinement effects every single quantum dot has its own characteristic emission wavelength, which is determined by the size of the quantum dot. Due to the large size distribution the emission spectrum of an ensemble of CdSe/ZnS quantum dots is extensively broadened compared to the emission spectrum of a single quantum dot.

An example of a spectrally resolved time-trace is shown in Fig. 19.5a. Apparently and, we must stress, exceptionally, two different quantum dots were present in the detection volume of the spectrograph-CLSM set-up, clearly separated due to their different emission wavelengths, i.e., 605 and 560 nm, respectively. Spectra at time marks I, II, and III are shown in Fig. 19.5b. Clearly, the emission intensity of the two QDs differs. In addition, the blinking behavior is apparent, and also, both QDs blink independently.

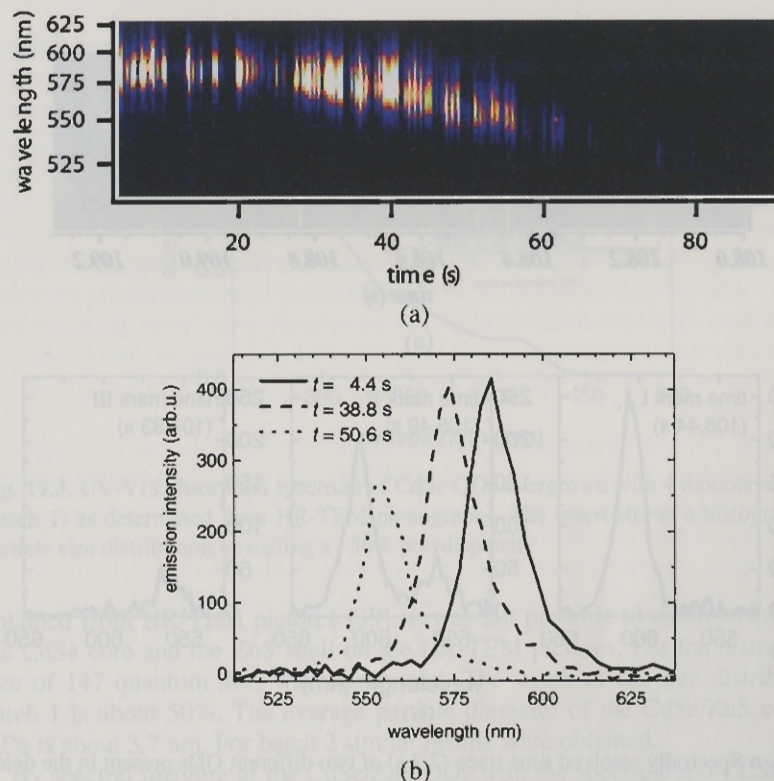


Fig. 19.6. Spectrally resolved time trace **a** of a CdSe/ZnS QD of batch 1 in ambient air present in the detection volume of the spectrograph-CLSM set-up (excitation at 468 nm, room temperature). Note that the intensity is a stretched false color representation. Emission spectra at different illumination times are shown in **b**

Luminescence spectra of individual CdSe/ZnS quantum dots were measured for a large number of quantum dots. Clear differences are observed between the time evolutions of the emission spectra of the quantum dots, even for dots of the same batch in the same atmosphere. To obtain reliable information on the influence of the atmosphere and the thickness of the capping layer on the spectral diffusion and on/off behavior, the emission spectra of 41 different dots were followed in time. In Fig. 19.6a a typical spectrally resolved time trace (duration 80 s) is presented of a CdSe/ZnS QD of batch 1 in *air*. Initially this QD emits at 585 nm (for about 20 s), and then the emission wavelength starts to shift to the blue. After a blue shift of about 40 nm the emission of the QD is fully photo-bleached. A blow-up of a smaller part of the time trace (not shown) shows blinking of the QD, see [42]. Figure 19.6b shows spectra of the dot collected (6 ms integration) at different times. It is clear that the two spectra recorded at the later times are blue shifted with respect to the initial wavelength. The FWHM of the peaks is about 15 nm. The result of fitting of the emission maxima is shown in Fig. 19.7a, where the

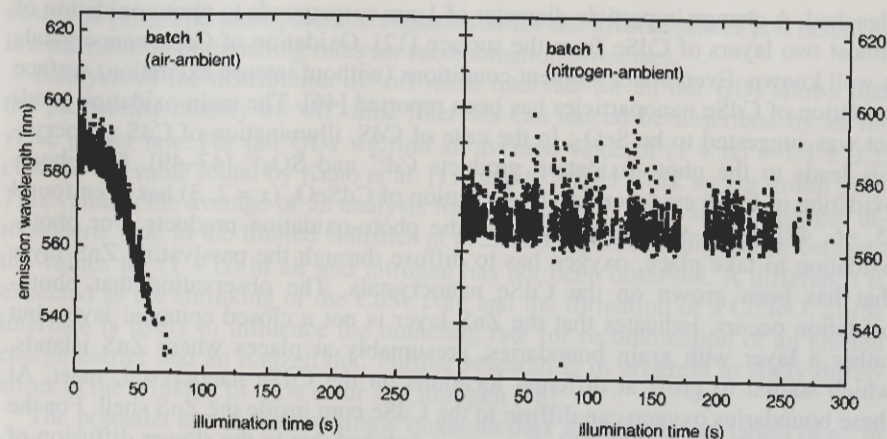


Fig. 19.7. Emission wavelength as a function of time of the CdSe/ZnS QD of Fig. 19.6, i.e., batch 1 in air (a) and of a CdSe/ZnS QD of batch 1 in a nitrogen atmosphere (b)

emission wavelength of a CdSe/ZnS QD from batch 1 in *air* is depicted as a function of time. Similar results are obtained for other quantum dots of batch 1 and 2 in *air*, with a blue shift of 29 ± 10 nm and 29 ± 17 nm, respectively, before the luminescence disappears. In some cases an initial fast blue shift is observed, while for most QDs a behavior similar to that depicted in Fig. 19.7a is observed [36]. For QDs of batch 1, the luminescence intensity decreases in time and no luminescence is observed after typically 2.5 minutes. There are large differences between quenching times for individual dots, in agreement with previously reported results [12]. Due to the increased thickness of the passivating ZnS layer for QDs from batch 2, the time scales for the blue shift and the photobleaching are significantly longer (bleaching occurs on average after 3.5 minutes).

The time-evolution of the fitted emission wavelength for a single CdSe/ZnS QD of batch 1 in *nitrogen* atmosphere is depicted in Fig. 19.7b. Clearly, no blue shift is observed. The emission wavelength of this QD varies around an average value of about 570 nm (Fig. 19.7b). A spectral variation of about 10 nm is observed. This is in agreement with previous measurements, which show that over longer time periods random spectral diffusion can result in shifts of up to 10 nm [43,44]. *Contrary* to the situation in *air*, there is only random spectral diffusion in time and no shift to shorter wavelengths is observed. The time periods for which the dots show emission (until photobleaching occurs) are significantly longer for the QDs in *nitrogen* than in *air* (about 10 minutes on average for both batches).

The observed differences between the time evolution of the emission spectra of single quantum dots in *air* and in *nitrogen* provide convincing evidence that the observed blue shift of the emission in *air* is due to photo-oxidation of CdSe [45]. From the blue shift and the well-known relation between bandgap and the diameter of CdSe particles [2, 5–7] it can be calculated that the effective CdSe core diameter decreases from about 5 nm to about 4 nm before the dot is completely

bleached. A change in particle diameter of 1 nm corresponds to photo-oxidation of almost two layers of CdSe from the surface [12]. Oxidation of CdSe nanocrystals is well known. Even under ambient conditions (without intense excitation) surface oxidation of CdSe nanoparticles has been reported [46]. The main oxidation product was suggested to be SeO_2 . In the case of CdS, illumination of CdS nanocrystals leads to the photo-oxidation products Cd^{2+} and SO_4^{2-} [47–49]. For photo-oxidation of CdSe evidence for the formation of CdSeO_x ($x = 2, 3$) has been found [5, 46, 47]. Here, we did not analyze the photo-oxidation products. For photo-oxidation to take place, oxygen has to diffuse through the passivating ZnS layer that has been grown on the CdSe nanocrystals. The observation that photo-oxidation occurs, indicates that the ZnS layer is not a closed epitaxial layer, but rather a layer with grain boundaries, presumably at places where ZnS islands, which started to grow at different locations on the CdSe nanocrystal, meet. At these boundaries oxygen can diffuse to the CdSe core inside the ZnS shell. For the thicker shell (batch 2) the oxidation rate is reduced due to the slower diffusion of oxygen to the CdSe core through a thicker ZnS shell.

As a result of the photo-oxidation at the CdSe surface, quenching states are expected to be formed at the CdSe/CdSeO_x interface. The formation of surface quenching states causes a decrease of the number of photons emitted. In the single QD emission spectra a gradual decrease in light output is indeed observed as the emission shifts to shorter wavelengths. Finally, the luminescence disappears and the QD has bleached. The occurrence of photo-oxidation for QDs can explain the shorter bleaching times observed for QDs in *air*. Also in a *nitrogen* atmosphere photobleaching occurs, albeit after much longer times. In view of the high laser power (20 kW/cm²) photobleaching is not unexpected. Few materials are stable against photodegradation under the presently used laser power. The nature of the photo-induced quenching states is not clear. The efficiency of the photo-induced formation of quenching states in *nitrogen* is much lower than for photo-oxidation observed in *air*. Possibly, a high-energy bi-exciton state in a single dot has enough energy to rearrange or break bonds at the CdSe/ZnS interface, which gives rise to non-radiative recombination channels and finally leads to bleaching.

The blinking behavior of the ZnS coated CdSe QDs can also be studied from the spectral time-traces as shown in Fig. 19.6. The emission intensity was used as a means to distinguish between an 'on' and an 'off' state of the QD. A threshold set just above the background was determined to discriminate between 'on' and 'off' state. Blinking can be quantified by thus determining the 'off' and 'on' time distributions. Blinking behavior of ZnS coated CdSe QDs has been studied in detail by Kuno et al. [13]. Evidence was provided for an inverse power law behavior of the off-time intervals, i.e., $P(t_{\text{off}}) \propto t_{\text{off}}^{-(1+\alpha)}$. A good agreement between the experimentally observed off-time distribution over nine decades in probability density and five decades in time was observed, with $(1 + \alpha) = 1.6 \pm 0.2$. Since the process that leads to the off state is assigned to photo-ionization (by an Auger process) of the QD, the off-time intervals are related to recombination of the ejected charge carrier with the ionized dot. As a result the off-time interval distribution is expected to be excitation intensity independent, which has indeed been

observed [13]. The most probable explanation for the inverse power law behavior is a distribution of tunneling rates for recombination processes.

Analysis of the distribution of 'off'-time intervals for all our QDs shows that the probability density of 'off'-time intervals can indeed be described by an inverse power law. For our QDs we find an average value of $(1 + \alpha) = 1.4 \pm 0.2$, close to the value found by Kuno et al. [13] and to earlier work by our group [50]. This value is the average of an analysis for 41 QDs, both in air and in nitrogen atmosphere. Due to the limited statistics at present a significant difference between the values for $(1 + \alpha)$ in air and nitrogen has not been observed. A difference is expected as the shrinking of the CdSe core and the formation of a CdSeO_x at the interface is likely to influence the tunneling rate for recombination of an ejected charge carrier and an ionized dot. Further research is in progress to study differences in the blinking of QDs in air and nitrogen [38].

The potential application of single quantum dots as luminescent labels (e.g., in biological systems) is based on the high stability in combination with a relative narrow emission band and a large 'Stokes shift' [10, 15]. The total number of photons emitted by a single QD until bleaching occurs is an important number. For single dye molecules (e.g., rhodamine [51–53]) the highest number of photons emitted before bleaching is around 10^6 at room temperature. Based on an overall efficiency of about 5% for the system (i.e., one out of every twenty emitted photons is counted), the number of photons emitted by a single QD before bleaching occurs, is typically 2×10^7 , with numbers exceeding 10^8 for the more robust quantum dots. These numbers are more than an order of magnitude higher than for single dye molecules, which reflects the higher stability of inorganic chromophores such as semiconductor QDs.

Surprisingly, the total number of photons emitted before bleaching occurs is not much less for QDs in air than for QDs in nitrogen. The shorter lifetime of QDs in air is compensated for by a higher initial photon count in air. The initial emission intensity is about two times higher for QDs in air (about 3000 counts in air vs. 1500 counts in nitrogen during the 6 ms integration period for the brightest QDs). At present further experiments are conducted to provide more precise information on the difference in initial light output. A possible explanation for the higher initial light output in air is quenching of QD defect luminescence by oxygen. It is well known that in addition to the fast (nanosecond) exciton emission, also relatively long-lived (microsecond) defect emission can occur in QDs [47, 54]. Due to the long lifetime, the fast photon absorption and emission process is interrupted, until the long-lived excited state has returned (via radiative or non-radiative relaxation) to the ground state. If oxygen can quench the defect luminescence, a higher exciton emission yield is expected by reduction of the time spent in the 'dark state'. For CdSe we have not found studies on the role of oxygen on the efficiency of the defect emission. For other II–VI semiconductors like CdS and ZnS it has been established that oxygen can quench the defect-related emission [47, 54]. If the same occurs for CdSe QDs, this can explain the higher initial light output observed for CdSe QDs in air. The presently applied excitation power (20 kW/cm²) yields initial intensities of 1000–3000 counts in 6 ms. Assuming a 5% collection efficiency, this corresponds to time intervals of 100–300 ns between

emission of photons. In this situation relaxation to a trap state with a microsecond lifetime will reduce the number of photons emitted and a fast return to the ground state by non-radiative relaxation enhances the photon output. A similar situation has been reported for dye molecules where higher fluorescence light yields were measured by quenching of the triplet state luminescence [55].

19.4 Conclusion

In this chapter, we have described a highly sensitive home-built spectrograph that is optimized for use in (scanning) fluorescence microscopy. It has been designed such that it can be easily retrofitted to any commercially available CLSM. At present the time-resolution is limited by the CCD-camera and amounts to 1.2 ms. Fast spectral imaging is possible up to a rate of 800 spectra per second. This is of great importance in biological studies, where one wants to follow protein-protein reaction/interaction kinetics on a sub-second timescale.

As an example of the versatility in use of the spectrograph-CLSM set-up time-resolved luminescence experiments on single CdSe/ZnS core-shell quantum dots were shown. A large blue shift in the emission wavelength of about 30 nm was observed for QDs in ambient air. In contrast, this shift was not observed for QDs in a nitrogen atmosphere. Moreover, the bleaching time and initial emission intensity of single QDs were influenced by the presence of oxygen. The results were explained by photo-induced oxidation of the CdSe crystallites.

Acknowledgements. We thank Cees van der Oord for additional programming, Ageeth Bol and Joost van Lingen for QD synthesis. Further, we gratefully acknowledge the Netherlands Technology Foundation (STW) and the Netherlands Council for Earth and Life Sciences (ALW) of the Netherlands Organization for Scientific Research (NWO) for financial support.

References

1. Alivisatos AP (1996) Perspectives on the physical chemistry of semiconductor nanocrystals. *J Phys Chem* 100:13226–13239
2. Gaponenko SV (1998) Optical properties of semiconductor nanocrystals. Cambridge University Press, Cambridge, U.K.
3. Efros AIL, Rosen M (2000) The electronic structure of semiconductor nanocrystals. *Annu Rev Mater Sci* 30:475–521
4. Yoffe AD (2001) Semiconductor quantum dots and related systems: electronic, optical, luminescence and related properties of low dimensional systems. *Adv Phys* 50:1–208
5. Dabbousi BO, Rodriguez-Viejo J, Mikulec FV, Heine JR, Mattoussi H, Ober R, Jensen KF, Bawendi MG (1997) (CdSe)ZnS core-shell quantum dots: synthesis and characterization of a size series of highly luminescent nanocrystallites. *J Phys Chem B* 101:9463–9475

6. Empedocles S, Bawendi MG (1999) Spectroscopy of single CdSe nanocrystallites. *Acc Chem Res* 32:389–396
7. Mikulec FV, Kuno M, Bennati M, Hall DA, Griffin RG, Bawendi MG (2000) Organometallic synthesis and spectroscopic characterization of manganese-doped CdSe nanocrystals. *J Am Chem Soc* 122:2532–2540
8. Nanotech, special issue. (2001) *Scientific American* 285 (3)
9. Hines MA, Guyot-Sionnest P (1996) Synthesis and characterization of strongly luminescent ZnS-capped CdSe nanocrystals. *J Phys Chem* 100:468–471
10. Bruchez Jr. M, Moronne M, Gin P, Weiss S, Alivisatos AP (1998) Semiconductor nanocrystals as fluorescent biological labels. *Science* 281:2013–2016
11. Blanton SA, Dehestani A, Lin PC, Guyot-Sionnest P (1994) Photoluminescence of single semiconductor nanocrystallites by two-photon excitation microscopy. *Chem Phys Lett* 229:317–322
12. Nirmal M, Dabbousi BO, Bawendi M, Macklin JJ, Trautmann JK, Harris TD, Brus LE (1996) Fluorescence intermittency in single cadmium selenide nanocrystals. *Nature* 383:802–804
13. Kuno M, Fromm DP, Hamann HF, Gallagher A, Nesbitt DJ (2000) Nonexponential “blinking” kinetics of single CdSe quantum dots: a universal power law behavior. *J Chem Phys* 112:3117–3120
14. Kuno M, Fromm DP, Hamann HF, Gallagher A, Nesbitt DJ (2001) “On”/“off” fluorescence intermittency of single semiconductor quantum dots. *J Chem Phys* 115:1028–1040
15. Chan WCW, Nie S (1998) Quantum dot bioconjugates for ultrasensitive nonisotopic detection. *Science* 281:2016–2018
16. Dahan M, Laurence T, Pinaud F, Chemla DS, Alivisatos AP, Sauer M, Weiss S (2001) Time-gated biological imaging by use of colloidal quantum dots. *Opt Lett* 26:825–827
17. Gerion D, Pinaud F, Williams SC, Parak WJ, Zanchet D, Weiss S, Alivisatos AP (2001) Synthesis and properties of biocompatible water-soluble silica-coated CdSe/ZnS semiconductor quantum dots. *J Phys Chem B* 105:8861–8871
18. Efros AIL, Rosen M (1997) Random telegraph signal in the photoluminescence intensity of a single quantum dot. *Phys Rev Lett* 78:1110–1113
19. Banin U, Bruchez M, Alivisatos AP, Ha T, Weiss S, Chemla DS (1999) Evidence for a thermal contribution to emission intermittency in single CdSe/CdS core/shell nanocrystals. *J Chem Phys* 110:1195–1201
20. Neuhauser RG, Shimizu KT, Woo WK, Empedocles SA, Bawendi MG (2000) Correlation between fluorescence intermittency and spectral diffusion in single semiconductor quantum dots. *Phys Rev Lett* 85:3301–3304
21. Empedocles SA, Bawendi MG (1997) Quantum-confined stark effect in single CdSe nanocrystallite quantum dots. *Science* 278:2114–2117
22. Cordero SR, Carson PJ, Estabrook RA, Strouse GF, Buratto SK (2000) Photo-activated luminescence of CdSe quantum dot monolayers. *J Phys Chem B* 104:12137–12142
23. Tsien RY, Poenie M (1986) Fluorescence ratio imaging: a new window into intracellular ionic signaling. *Trends Biochem Sci* 11:450–455
24. Matyus L (1992) New trends in photobiology. *J Photochem Photobiol B: Biol* 12:323–337
25. Willard DM, Carillo LL, Jung J, Van Orden A (2001) CdSe-ZnS quantum dots as resonance energy transfer donors in a model protein-protein binding assay. *Nano Lett* 1:469–474

26. Gordon GW, Berry G, Liang XH, Levine B, Herman B (1998) Quantitative fluorescence resonance energy transfer measurements using fluorescence microscopy. *Biophys J* 74:2702–2713
27. Feofanov A, Sharonov S, Valisa P, Da Silva E, Nabiev I, Manfait M (1995) A new confocal stigmatic spectrometer for micro-Raman and microfluorescence spectral imaging analysis: design and application. *Rev Sci Instrum* 66:3146–3158
28. Millot J-M, Pingret L, Angiboust J-F, Bonhomme A, Pinon J-M, Manfait M (1995) Quantitative determination of free calcium in subcellular compartments, as probed by Indo-1 and confocal microspectrofluorometry. *Cell Calc* 17:354–366
29. Martínez-Zaguilán R, Gurulé MW, Lynch M (1996) Simultaneous measurement of intracellular pH and Ca^{2+} in insulin-secreting cells by spectral imaging microscopy. *Am J Physiol* 270:C1438–C1446
30. Vereb G, Jares-Erijman E, Selvin PR, Jovin TM (1998) Temporally and spectrally resolved imaging microscopy of lanthanide chelates. *Biophys J* 74:2210–2222
31. Favard C, Valisa P, Egret-Charlier M, Sharanov S, Herben C, Manfait M, Da Silva E, Vigny P (1999) A new UV-visible confocal laser scanning microspectrofluorometer designed for spectral cellular imaging. *Biospectrosc* 5:101–115
32. Rigacci L, Alterini R, Bernabei PA, Ferrini PR, Agati G, Fusi F, Monici M (2000) Multispectral imaging autofluorescence microscopy for the analysis of lymph-node tissues. *Photochem Photobiol* 71:737–742
33. Lacoste TD, Michalet X, Pinaud F, Chemla DS, Alivisatos AP, Weiss S (2000) Ultra-high-resolution multicolor colocalization of single fluorescent probes. *Proc Natl Acad Sci USA* 97:9461–9466
34. Tsurui H, Nishimura H, Hattori S, Hirose S, Okumura K, Shirai T (2000) Seven-color fluorescence imaging of tissue sample based on fourier spectroscopy and singular value decomposition. *J Histochem Cytochem* 48:653–662
35. Frederix PLTM, Asselbergs MAH, Van Sark WGJHM, Van den Heuvel DJ, Hamelink W, De Beer EL, Gerritsen HC (2001) High sensitivity spectrograph for use in fluorescence microscopy. *Appl Spec* 55:1005–1012
36. Frederix PLTM (2001) Spectral analysis in microscopy: A study of FRET and single quantum dot luminescence. Ph.D. Thesis, Utrecht University
37. Born M, Wolf E (1999) Principles of optics. Cambridge University Press, Cambridge, U.K.
38. Van Sark WGJHM, Frederix PLTM, Bol AA, Van den Heuvel DJ, Gerritsen HC, Meijerink A (2002) Blinking, blueing, and bleaching of single CdSe/ZnS quantum dots. *Phys Chem Chem Phys* (submitted)
39. Bol AA (2001) Luminescence of doped semiconductor quantum dots. Ph.D. Thesis, Utrecht University
40. Yen WM, Shionoya S (1999) Phosphor handbook. CRC Press, Boca Raton, FL
41. Li X-Q, Arakawa Y (1999) Optical linewidths in an individual quantum dot. *Phys Rev B* 60:1915–1920
42. Van Sark WGJHM, Frederix PLTM, Van den Heuvel DJ, Gerritsen HC, Bol AA, Van Lingen JNJ, De Mello Donegá C, Meijerink A (2001) Photo-oxidation and photobleaching of single CdSe/ZnS quantum dots probed by room-temperature time-resolved spectroscopy. *J Phys Chem B* 105:8281–8284
43. Blanton SA, Hines MA, Guyot-Sionnest P (1996) Photoluminescence wandering in single CdSe nanocrystals. *Appl Phys Lett* 69:3905–3907

44. Empedocles SA, Neuhauser R, Shimizu K, Bawendi MG (1999) Photoluminescence from single semiconductor nanostructures. *Adv Mater* 11:1243–1256
45. Van Sark WGJHM, Frederix PLTM, Van den Heuvel DJ, Bol AA, Van Lingen JNJ, De Mello Donegá C, Gerritsen HC, Meijerink A (2001) Time-resolved fluorescence spectroscopy study on the photo-physical behaviour of quantum dots. *J Fluorescence* 12:69–76
46. Bowen Katari JE, Colvin VL, Alivisatos AP (1994) X-ray photoelectron spectroscopy of CdSe nanocrystals with applications to studies of the nanocrystal surface. *J Phys Chem* 98:4109–4117
47. Henglein A (1988) Mechanism of reactions on colloidal microelectrodes and size quantification effects. *Top Curr Chem* 143:113–180
48. Dunstan DE, Hagfeldt A, Almgren M, Siegbahn HOG, Mukhtar E (1990) Importance of surface reactions in the photochemistry of ZnS colloids. *J Phys Chem* 94:6797–6804
49. Spanhel L, Haase M, Weller H, Henglein A (1987) Photochemistry of colloidal semiconductors. 20. Surface modification and stability of strong luminescing CdS particles. *J Am Chem Soc* 109:5649–5655
50. Van Sark WGJHM, Frederix PLTM, Van den Heuvel DJ, Asselbergs MAH, Senf I, Gerritsen HC (2000) Fast imaging of single molecules and nanoparticles by wide-field microscopy and spectrally resolved confocal microscopy. *Single Mol* 1:291–298
51. Rosenthal I (1978) Photochemical properties of rhodamine 6G in solution. *Opt Comm* 24:164–166
52. Huston AL, Reimann CT (1991) Photochemical bleaching of adsorbed rhodamine 6G as a probe of binding geometries on a fused silica surface. *Chem Phys* 149:401–407
53. Schmidt Th, Schütz GJ, Baumgartner W, Gruber HJ, Schindler H (1996) Imaging of single molecule diffusion. *Proc Natl Acad Sci USA* 93:2926–2929
54. Chestnoy N, Harris TD, Hull R, Brus LE (1986) Luminescence and photophysics of CdS semiconductor clusters: the nature of the emitting electronic state. *J Phys Chem* 90:3393–3399
55. Song L, Varma CAGO, Verhoeven JW, Tanke HJ (1996) Influence of the triplet excited state on the photobleaching kinetics of fluorescein in microscopy. *Biophys J* 70:2959–2968